IEEE Access
Multidisciplinary | Rapid Review | Open Access Journal

Received June 23, 2020, accepted July 6, 2020, date of publication July 9, 2020, date of current version July 22, 2020.

Digital Object Identifier 10.1109/ACCESS.2020.3008166

Sparse Nonuniform Frequency Sampling for Fast SFCW Radar Imaging

WEIKANG SI, XIAODONG ZHUGE, AND JUNGANG MIAO
School of Electronics and Information Engineering, Beihang University, Beijing 100191, China

Corresponding author: Xiaodong Zhuge (zhuge@buaa.edu.cn)

This work was supported in part by the two Key Programs of the National Natural Science Foundation of China under Project 41531175 and Project 61731001, in part by the Beihang Hundred Talents Plan, and in part by the Beihang Top Young Scholars Program.

ABSTRACT Stepped frequency continuous wave (SFCW) radar achieves wide bandwidth by synthesizing series of monochromatic pulses in a consecutive manner. Uniform frequency sampling is often performed with a constant frequency step, which in turn limits the maximum unambiguous range achievable by the radar to reliably distinguish targets. Thus, a small frequency step must be selected when clutters exist at long distances even though the target of interests is located at much closer distances. This is costly since a large number of frequencies must be synthesized, which leads to slow acquisition speed. In this paper, a sparse nonuniform frequency sampling method is proposed to effectively reduce the number of frequencies while suppressing aliasing effects from clutters. The Poisson Sum Formula is utilized to derive a deterministic formula for choosing a discrete set of frequencies within a specified frequency band. A corresponding frequency weighting formula is added in order to maintain the same target impulse response in time-domain as the one achieved by dense uniform frequency sampling. Numerical and experimental results are presented to demonstrate the improved performances of the proposed sparse sampling method for SFCW radar imaging.

INDEX TERMS Nonuniform frequency sampling, Poisson sum formula, sparse sampling, stepped frequency continues wave.

I. INTRODUCTION

Due to large dynamic range, high phase accuracy and stable system performances, SFCW radar is widely used in many applications, such as through-wall radar, concealed weapon detection and non-destructive testing [1]–[5]. Traditional SFCW scheme includes a series of amplitude-phase measurements acquired at equally spaced frequency points, and corresponding time-domain signal or range profile is obtained by taking inverse Fourier transform (IFT) on the frequency-domain data. Thus, the Maximum unambiguous range (MUR) is limited by the frequency step Δf in SFCW

$$R_{MUR} = c/2\Delta f \tag{1}$$

where c is the speed of propagation. If an object is located outside the MUR, its time-domain response will be folded inside after IFT due to aliasing effects from insufficient frequency sampling. This is illustrated in Figure. 1 where objects located outside MUR appears as clutters and can possibly overlap with real target response. It is especially a big problem when performing short-range imaging of targets in a complex environment. Although the region of interests is quite small, very fine frequency step must be used in order to avoid the influence of background objects from far distances. Under a constant bandwidth, finer step leads to more frequency sampling points and long acquisition time, which is unacceptable in many applications that requires fast or even real-time imaging. Therefore, effective solutions are needed to allow sparse sampling while reducing aliasing effects.

Possible hardware solution involves employing additional RF switch at the receiver, which can reject unwanted clutters by time-gating. Currently the off-the-shelf solid-state switch has a switch time on the order of 100ns. Thus, it is a viable solution only when the separation between the target and clutters are large enough (e.g. at least 15m). Other strategies for increasing ambiguity range are based on random frequency sampling. The effect of random sampling for SFCW radar was analyzed in [6]. It is shown that the ambiguity in range could be suppressed, however, a noise

The associate editor coordinating the review of this manuscript and approving it for publication was Abhishek K Jha.

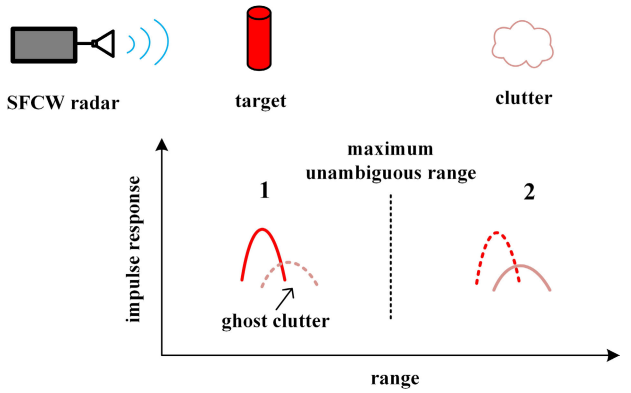

FIGURE 1. Illustration of aliasing effects when clutter is located outside the maximum unambiguous range due to insufficient frequency sampling in SFCW.

component is added to the range/Doppler sidelobes. In the field of ground penetrating radar and SAR imaging, random sparse sampling has been used together with compressive sensing (CS) techniques [1], [7]. This has shown good results in terms of reconstruction quality under specific conditions with the cost of high computational complexity. Random sampling was also applied with success for high-frequency surface imaging when the range extension of the target is smaller than the maximum unambiguous range [9]. Coprime sampling method has been applied in signal spectrum estimation and SAR imaging [10], [11]. A pair of coprime arrays can be used to sample a signal sparsely, and then reconstruct the autocorrelation at a significantly denser set of points. Thus, all applications based on autocorrelation can benefit from this technique. A nonuniform SFCW approach based on quadratic frequency spacing was proposed in [12] to reduce the maximum level of ambiguities for short-range imaging. There are also related literatures in the field of antenna array that addresses a similar sampling problem. In the far-field, the array factor is related to the array sampling via a Fourier transform. There, unequally spaced antenna arrays are proposed to suppress the effect of grating lobes [13], [14]. The basic theory of unequally spaced arrays based on Poisson sum formula is established in [16] with detailed discussion on its use in thinned array configurations. The stationary phase method was used to quantitatively analyze antenna patterns in different array distributions [15]–[18].

In this paper, a deterministic sparse frequency sampling method is proposed to suppress aliasing effects from clutters. By imposing a flat ambiguity plateau and unchanged impulse response, a weighted square-root frequency distribution can be derived based on the established method of Poisson sum formula [16]. Both numerical and measurement results illustrate that this method is effective in reducing the influence of clutters outside the maximum unambiguous range. It is particularly effective in achieving high quality imaging with sparse frequency sampling under a complex environment.

The rest of this paper is organized as follows. Section II formulates the treatment of range ambiguity in frequency sampling and introduces the proposed sampling method as well as related frequency weighting formula. Numerical and experimental results are presented and analyzed in Section III. Finally, Section IV summarizes the results and conclusions of this paper.

II. FORMULATIONS

In this section, the proposed sparse nonuniform frequency sampling distribution is formulated. Assuming N frequencies are acquired by a SFCW radar, the received signal in frequency-domain at the n^{th} frequency from a point-like target can be formulated as

$$s[n] = \sigma \cdot I[n]\, e^{-j2\pi f[n]\tau} \tag{2}$$

where σ and τ are the reflectivity and time delay of the target, and $f[n]$ and $I[n]$ represent the frequencies and amplitudes of the SFCW measurements. The corresponding time-domain signal can be obtained via discrete inverse Fourier transform (IDFT)

$$s(t) = \frac{1}{N}\sum_{n=1}^{N} s[n] e^{j2\pi f[n]t} \tag{3}$$

Under conventional SFCW, the frequencies are equally spaced, then f can be expressed as

$$f[n] = f_s + (n-1)\,\Delta f \tag{4}$$

with f_s represents the starting frequency, and Δf is the step between neighboring frequencies. Substituting (4) into (2) results in

$$s[n] = \sigma \cdot I[n]\, e^{-j2\pi[f_s+(n-1)\Delta f]\tau} \tag{5}$$

Equation (5) shows that under periodic sampling when the time-delay of the target τ equals the integer times of $1/\Delta f$, the acquired frequency-domain data would exhibit ambiguities due to phase wrapping.

To avoid this, controlled aperiodicity should be introduced. In order to arrive at a deterministic formula for the nonuniform frequency distribution, the Poisson sum formula is utilized to connect discrete sums with continuous integrals. The Poisson sum has the following form [19]

$$\sum_{n=-\infty}^{\infty} h[n] = \sum_{m=-\infty}^{\infty}\int_{-\infty}^{\infty} h(v) e^{-j2\pi mv} dv \tag{6}$$

Thus we rewrite (3) as

$$s(t) = \sum\nolimits_{m=-\infty}^{\infty} s_m(t) \quad m = 0, \pm 1, \pm 2, \cdots \tag{7}$$

where

$$\begin{aligned} s_m(t) &= \frac{1}{N}\int_{-\infty}^{\infty} s(v)\, e^{j2\pi[f(v)\text{t-mv}]} dv \\ &= \frac{\sigma}{N}\int_{-\infty}^{\infty} I(v) e^{j2\pi[f(v)(t-\tau)-mv]} dv \end{aligned} \tag{8}$$

Note that the frequency distribution $f(v)$ vanishes for $v \leq 0$ and $v > N$. Equation (8) gives the formula to relate the continuous Fourier transform with the discrete samples of the SFCW data. Under this formulation, the samples of $s_m(t)$ represent different parts of the time-domain response, with $s_0(t)$ corresponding to the main pulse from the actual target and $s_m(t)$ corresponding with the m^{th} ambiguity plateaus.

Equation (8) can be reformulated as

$$s_m(t) = \frac{\sigma}{N}\int_{-\infty}^{\infty} I[v]\, e^{j\varphi(v)} dv \tag{9}$$

where

$$\varphi(v) = 2\pi f(v)(t-\tau) - 2\pi m v \tag{10}$$

The integral in (9) can be expressed using the method of stationary phase (MSP) [20] as

$$s_m(t) = \frac{\sigma}{N} I(\bar{v}) \sqrt{\frac{2\pi}{\varphi''(\bar{v})}} e^{j\varphi(\bar{v})} e^{-j\frac{\pi}{4}} \tag{11}$$

where $\bar{v}$ are the points of stationary phase fulfilling the following equation

$$\varphi'(\bar{v}) = 2\pi f'(\bar{v})(t-\tau) - 2\pi m = 0 \tag{12}$$

The envelope of the ambiguity plateau in (11) can be expressed as

$$|s_m(t)| = \frac{\sigma}{N} I(\bar{v}) \sqrt{\frac{2\pi}{\varphi''(\bar{v})}} = \frac{\sigma}{N} I(\bar{v}) \sqrt{\frac{f'(\bar{v})}{m f''(\bar{v})}} \tag{13}$$

Equation (13) provides the relationship between the envelope of the resulting time-domain response or range profile and the first/second derivatives of the frequency distribution function at the points of stationary phase.

Based on this formulation, we can pursue a nonuniform frequency distribution that can fulfill requirements placed on the time-domain response. The first requirement is that the ambiguity plateau should be as flat as possible without any slope. This is useful since a flat background will be less likely to be recognized as target reflections. This requires the envelope to be a constant, thus

$$|s_m(t)| = \frac{\sigma}{N} I(\bar{v}) \sqrt{\frac{f'(\bar{v})}{m f''(\bar{v})}} = A_m \tag{14}$$

The second requirement is to maintain the same main impulse response for the actual target under sparse nonuniform frequency sampling as the one obtained from dense uniform sampling. From (8), we can perform a change of variable while setting $m = 0$. This results in

$$\begin{aligned} s_0(t) &= \frac{\sigma}{N}\int_{-\infty}^{\infty} I(v)\frac{dv}{df} e^{j2\pi f(v)(t-\tau)} df \\ &= \frac{\sigma}{N}\int_{-\infty}^{\infty} \frac{I(v)}{f'(v)} e^{j2\pi f(v)(t-\tau)} df \end{aligned} \tag{15}$$

Under uniform frequency sampling, the derivative of the sampling function is a constant, as $f'(n) = \Delta f$. But this is not the case for nonuniform sampling. Therefore, in order to obtain the same impulse response, the weighting of the frequencies should be introduced that satisfy the following relation

$$I(v) = f'(v) \tag{16}$$

This will cancel out the influence of the nonuniform frequency sampling on the main impulse response of the target.

Combining (16) with (14), we obtain the following equation

$$A_m^2 N^2 m f''(\bar{v}) - \sigma^2 \left[f'(\bar{v})\right]^3 = 0 \tag{17}$$

The solution to (17) can be written in the following form

$$f(\bar{v}) = f_s + \frac{B}{\gamma - 1}\left[\sqrt{\frac{(\gamma^2-1)\bar{v} + N}{N}} - 1\right] \tag{18}$$

where f_s is the start frequency, B is the bandwidth and γ is a coefficient. And the amplitude of the frequencies based on (16) should be

$$I(\bar{v}) = f'(\bar{v}) = \frac{B(\gamma+1)}{2N}\sqrt{\frac{N}{(\gamma^2-1)\bar{v} + N}} \tag{19}$$

From (18), we could also derive the formula for $f''(\bar{v})$

$$f''(\bar{v}) = \frac{B(\gamma+1)^2(\gamma-1)}{-4N^2}\left[\frac{(\gamma-1)^2\bar{v} + N}{N}\right]^{-\frac{3}{2}} \tag{20}$$

Using (14), we could derive the height of the ambiguity plateau under this nonuniform sampling scheme

$$|s_m(t)| = \sqrt{\frac{1}{2mN}\cdot\frac{\gamma+1}{\gamma-1}} \tag{21}$$

We name the nonuniform sampling scheme in (18) and (19) as weighted square-root frequency sampling due to its square-root relation with frequency index $\bar{v}$ and the corresponding requirement on the amplitude of the frequencies.

From (12) we can obtain the relation between $t-\tau$ and the stationary points

$$t - \tau = \frac{m}{f'(\bar{v})} \tag{22}$$

Thus, the expected extend of the m^{th} ambiguity plateau can be expressed as [9]

$$\frac{m}{[f'(\bar{v})]_{max}} \leq t - \tau \leq \frac{m}{[f'(\bar{v})]_{min}} \tag{23}$$

To ensure the smooth connection between the 1st and 2nd plateaus, the following condition must be met

$$\frac{1}{[f'(\bar{v})]_{min}} \leq \frac{2}{[f'(\bar{v})]_{max}} \tag{24}$$

This leads to the solution for the coefficient $\gamma \leq 2$. Therefore, under the condition that the first and second

ambiguity plateau are smoothly connected ($\gamma = 2$), the resulting frequency sampling scheme is further reduced to

$$f(\bar{v}) = f_s + B\left(\sqrt{\frac{3\bar{v}+N}{N}} - 1\right) \tag{25}$$

$$I(\bar{v}) = \frac{3B}{2N}\sqrt{\frac{N}{3\bar{v}+N}} \tag{26}$$

As the proposed frequency sampling is nonuniform, the time-domain response shall be calculated by IDFT or more efficiently by the Nonuniform Fast Fourier Transform (NUFFT) [21], [22] that combines the classical FFT with fast multipole method to achieve the $O(N \cdot logN)$ computational complexity. The results obtained in this paper uses the NUFFT kernel provided by an open-source Python implementation [23].

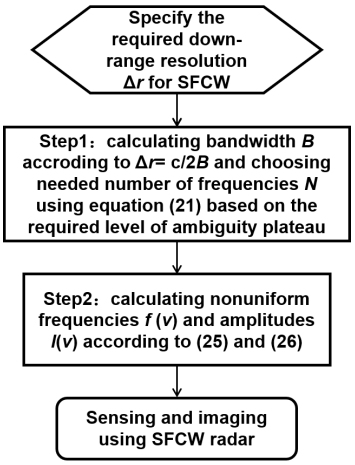

FIGURE 2. Flow chart illustration for the application of the proposed weighted square-root sampling method in SFCW sensing and imaging.

Figure 2 illustrates the use of the proposed nonuniform sampling scheme in SFCW sensing and imaging. Beginning with application requirements such as the needed down-range resolution, appropriate bandwidth and number of frequencies can be selected. Then equations (25) and (26) can be used to derive the list of frequencies and corresponding amplitudes under the proposed weighted square-root sampling scheme. After this, SFCW measurements can be carried out on the specified frequencies and amplitudes to achieve high-resolution sensing and imaging of targets with reduced aliasing effects from sparse sampling.

III. EXPERIMENTAL VERIFICATION

In this Section, simulation and measurement results are presented to verify the proposed formulations and sparse sampling technique.

A. NUMERICAL SIMULATIONS

Numerical simulations are performed first to verified the effectiveness of the proposed nonuniform sampling scheme.

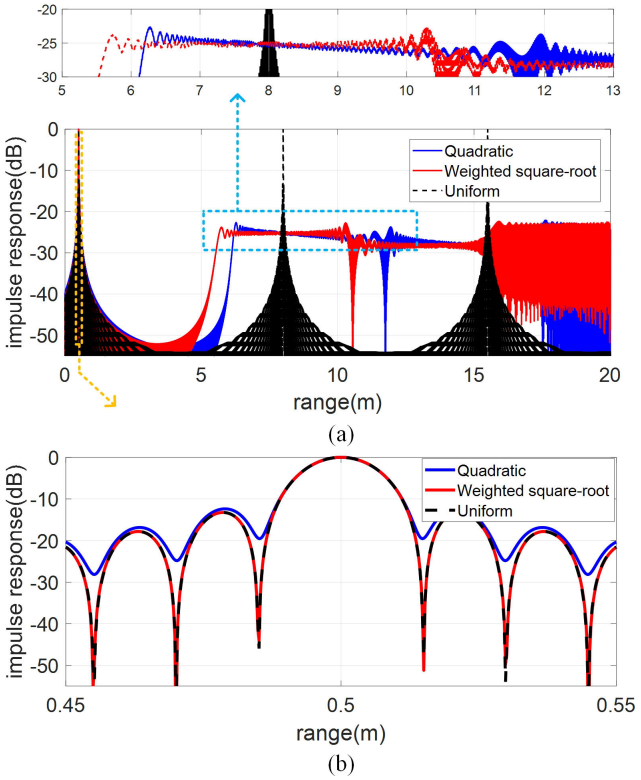

FIGURE 3. Comparison among time-domain impulse responses from uniform, quadratic and the proposed weighted square-root frequency sampling. (a) impulse responses of a single target at 0.5m distance, (b) the zoomed-out target impulse response. The simulated frequency band is 10 ∼ 20GHz with total frequency number N = 501.

Different sampling schemes are compared under the same number of frequencies using the same processing method. Figure 3 compares the time-domain signals obtained from uniform, quadratic and the proposed weighted square-root frequency sampling. The frequency band is from 10∼20GHz with the same 501 sampling points. A single point-like target is simulated at the distance of 0.5m from the radar. Under this setup, the frequency step for uniform sampling is 20MHz, resulting a MUR (maximum unambiguous range) of 7.5m. This is visible in Fig.3(a) where replications of the target response periodically appear and are separated by the MUR under uniform sampling. Both quadratic and the proposed sampling scheme provides a much lower ambiguity plateau at the level of −25dB from the maximum response from the target. As designed, the ambiguity plateau from weighted square-root is flat while the quadratic scheme exhibits a slop along the range distance. Fig.3(b) further compares the main impulse response for the target among three sampling methods. Quadratic sampling exhibits a higher sidelobe level and shallower depth of nulls. In comparison, the proposed method can deliver the same impulse response as the one provided by uniform sampling.

Due to larger maximum frequency step within the weighted square-root sampling under this scenario (30MHz vs. 26.7MHz), the separation between its ambiguity plateau

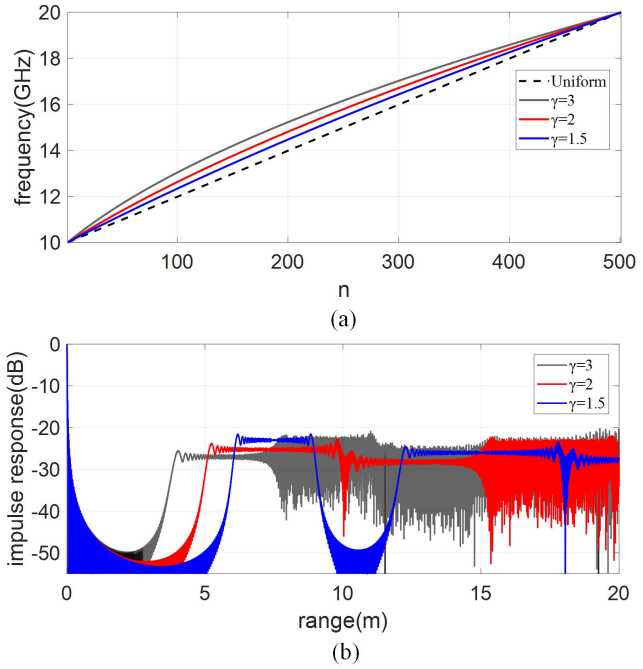

FIGURE 4. Study on the influence of coefficient γ. (a) frequency distributions under different choices of γ (e.g. $\gamma = 1.5$, 2 and 3), (b) time-domain impulse responses under different choices of γ.

and the target response is slightly smaller comparing with quadratic sampling. This can be adjusted by decreasing the coefficient γ. Figure 4 shows the influence of γ on the time-domain signals. Under the condition that $1 < \gamma < 2$, there is no overlap between the first and second order plateaus, and more separation between the first plateau and the target response can be created. As γ becomes larger, the envelope of the first-order plateau decreases while more overlap occurs among higher-order plateaus. Therefore, γ can be selected based on application requirements. When maximum separation to the target response is required, then γ should be configured to be close to 1. If a connected ambiguity plateau is needed, then γ should be equal or slightly smaller than 2 (e.g. 1.7∼2.0) to create acceptable mainlobe/plateau separation with connected flat ambiguity plateau.

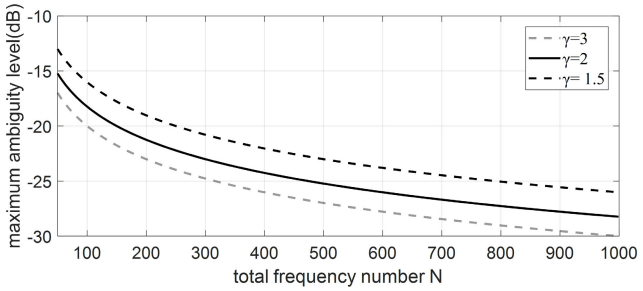

FIGURE 5. The variation of maximum amplitude of the ambiguity plateau with the number of frequency points N, when $\gamma = 1.5$, 2 and 3.

Figure 5 further plots the variation of the maximum amplitude of the ambiguity plateaus with the total number of frequency points under a fixed bandwidth for different choices of γ. It confirms the impact of γ on the maximum plateaus level. Furthermore, it shows the proposed nonuniform sampling method can still maintain a relative low level of ambiguities under small number of frequencies. A range ambiguity of -20dB can be achieved with only 100 frequency sampling points. This makes it a very effective sparse frequency sampling technique for fast SFCW sensing and imaging. It is worth noting that under a fixed frequency band, as the total frequency number increases, the maximum frequency interval decreases accordingly, which causes the ambiguity plateaus to move farther away from the target response in time-domain.

Figure 6 compares different sampling strategies under a typical near-field sensing scenario with clutters. A single target is located at 1m away from the radar, while clutters consisting of multiple point-like targets are distributed around 6m distance. The frequency band is between 10GHz and 20GHz with 351 sampling points. Four sampling strategies including uniform, random, quadratic and the proposed weighted square-root sampling are applied and compared with dense uniform sampling with 1001 sampling points. Because the MUR is 5.25m in uniform sparse sampling case, clutters appears symmetrically on both sides of the target with strong aliasing effects, as shown in Fig.6(a). All three nonuniform sampling strategies are able to effectively reduce the ambiguities from sparse sampling. The suppression of ambiguity is the weakest from random sampling with only 1.8dB reduction comparing with uniform sparse sampling. The proposed weighted square-root sampling provides the lowest ambiguity plateau among different sampling methods. Because of its property in terms of flat ambiguity plateau, weighted square-root sampling is able to maintain a relatively flat ambiguity plateaus even when many clutters exist. This is preferable under complex sensing scenarios. Quantitative comparison is further shown in Table 1. It is clear that the proposed method provides better sidelobe level (SLL), null depth and reduced ambiguity level than the other nonuniform sampling strategies.

TABLE 1. Quantitative comparison among different sampling methods.

	Sidelobe Level (dB)	Null Depth(dB)	Maximum level of Ambiguity Plateau
Uniform	-13.2	-37.5	-13.6
Random	-11.3	-23.5	-15.4
Quadratic	-10.7	-19.0	-22.2
Weighted square-root	-12.6	-28.4	-24.9

To further verify the effectiveness of the proposed method, near-field imaging simulation with point-like targets are performed. Figure 7 illustrates the target scenario used in the numerical simulation. The point-like targets are located on a cross-shaped grid with an interval of 0.05m, and placed at 1m distance from the antenna. Meanwhile, another cluster of targets are placed at 3.1m to simulate the effect of unwanted

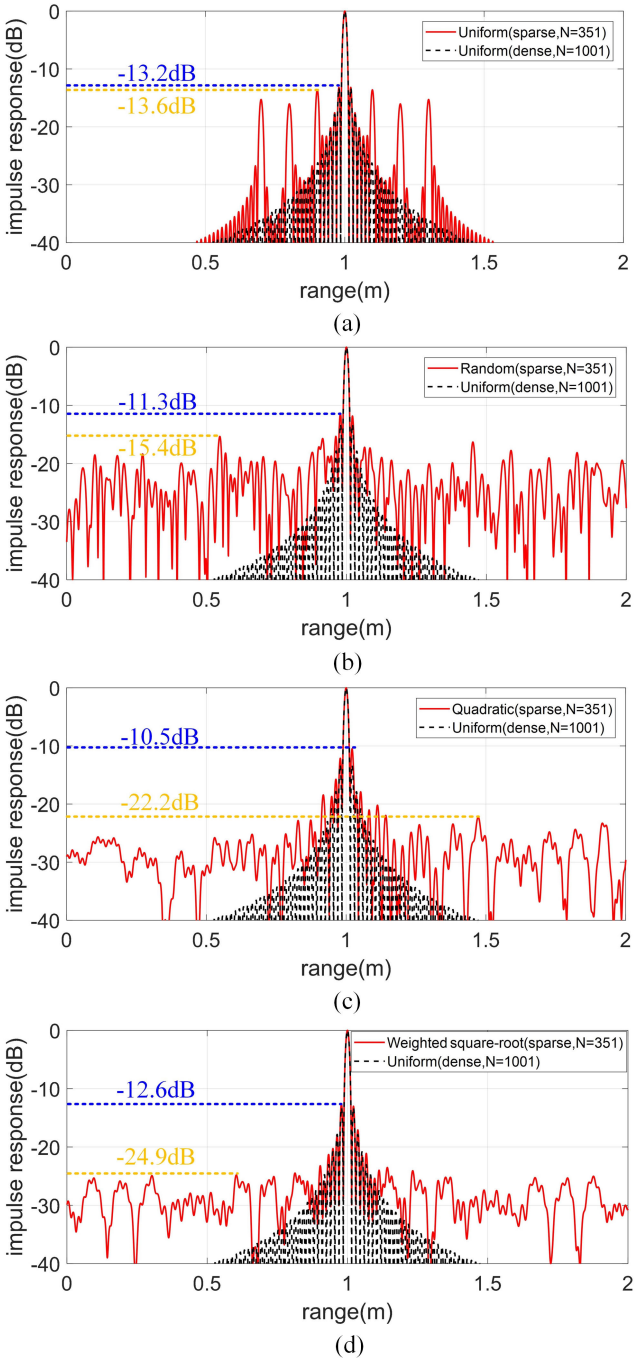

FIGURE 6. Comparison of sparse sampling strategies under strong clutters. A single point-like target is located at 1m from the radar, and the clutters are distributed between 5.95 to 6.55m. Dense uniform sampling (N = 1001) is used for comparison. Impulse responses from (a) uniform sampling, (b) random sampling,(c) quadratic sampling, and (d) the proposed weighted square-root sampling are compared.

clutters. A transmit/receive antenna pair scans across a planar aperture of 1m×1m with 1cm step. The antenna is assumed to be omnidirectional. Classical synthetic aperture radar imaging algorithm for rectilinear configuration is applied to obtain 3D images of the targets [24]. The frequency ranges from 10GHz to 24GHz with a total of 201 frequency points.

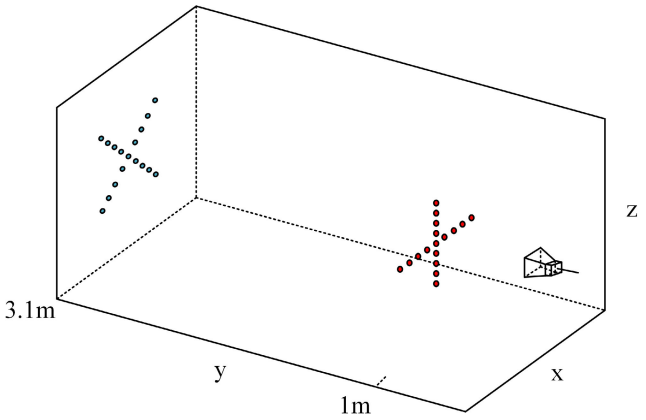

FIGURE 7. Illustration of simulated near-field imaging scenario with point-like targets located at 1m distance while clutters exists at 3.1m from the antenna aperture.

Under this configuration, the corresponding MUR is 2.143m under uniform frequency sampling. Therefore, the response from the target cluster at longer distance will overlap in time-domain with the one in front, and influence its imaging quality.

Figure 8 compares the imaging results of the targets at 1m distance between the uniform and the proposed weighted square-root frequency sampling. Both front and top views of the 3D images are created by maximum projection. The applied frequency sampling and weighting distributions are also shown. Although the ambiguous responses from clutters are mostly out-of-focus at target distances, it is visible that the result from uniform sampling is severely affected by objects outside the MUR with high background artifacts. In contrast, the images from the proposed sampling method show no degradation from clutters despite the sparse sampling condition.

B. MEASUREMENT RESULTS

The performances of the proposed nonuniform frequency sampling method are further verified by near-field SFCW imaging experiments using vector network analyzer (VNA). A ZVA24 VNA from Rohde & Schwarz is used to carry out the SFCW measurements. NI-VISA (Virtual Instrument Software Architecture) standard interface is used to control the VNA and to measure the specified sampling frequencies. The transmitted power and IF bandwidth of the VNA during experiment are 3dBm and 10KHz, respectively. Under this setting, the measurement time per frequency is approximately 0.5ms. Antipodal Vivaldi antennas are used as transmit/receive antennas that has an operational bandwidth from 2 to 26.5GHz and a 3dB beamwidth of about 75°(@15GHz) [25]. In the first experiment, the SFCW data from a standard metal sphere is acquired. The sphere is located at 0.68m in front of the antenna. The measurement frequency band is from 10GHz to 20GHz, the total frequency number is 501. Thus, the frequency step Δf is 20 MHz under uniform sampling, and the corresponding ambiguity range is

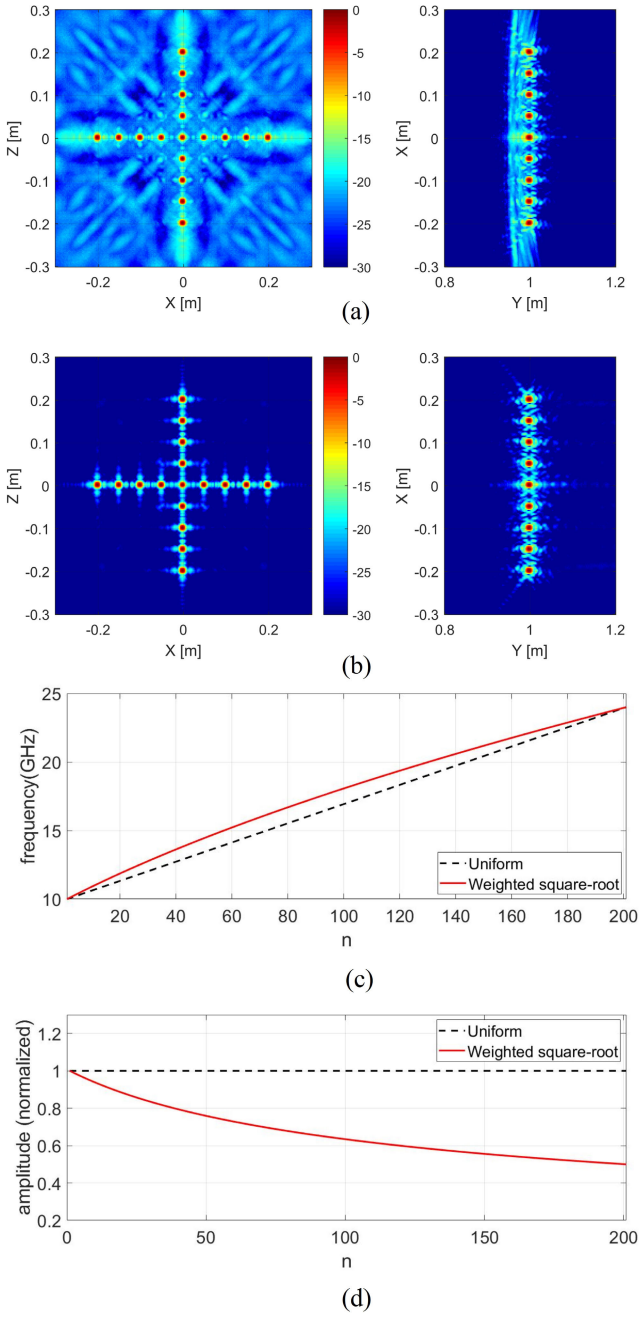

FIGURE 8. Comparison of imaging results of point-like targets under sparse frequency sampling. (a) reconstruction from uniform frequency sampling, (b) reconstruction from weighted square-root frequency sampling, (c) applied frequency distributions and (d) amplitudes for uniform and weighted square-root frequency samplings.

about 7.5 m. As shown in Figure 9, the ambiguity plateau of the weighted square-root sampling is approximately −25dB lower than uniform sampling. Its ambiguity plateau is almost flat as required. And the main target impulse response matches well between the uniform and nonuniform frequency distributions.

Two-dimensional synthetic aperture radar experiments are performed using a single transceiver pair mounted

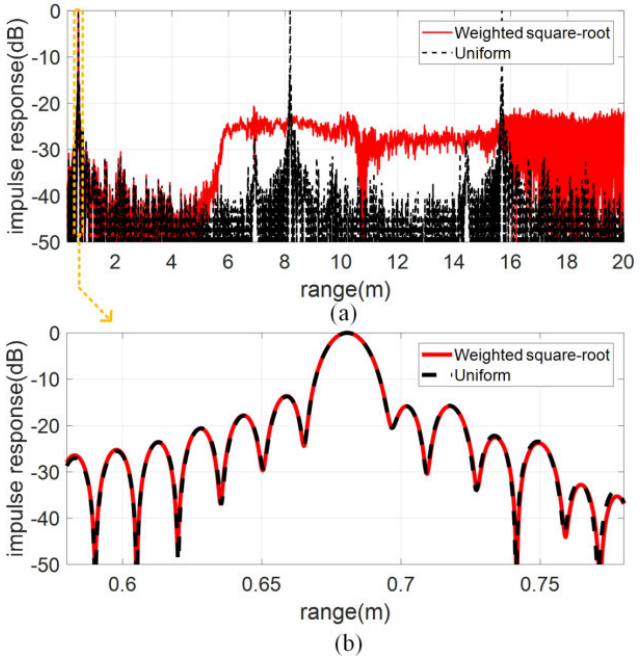

FIGURE 9. The measured time-domain impulse response of a metal sphere from uniform frequency sweep and the proposed weighted square-root sweep.

on a mechanical scanner. The test scenario is illustrated in Figure 10. Two resolution test patterns are measured at the distance of 1.2m from the antenna while having a wall 2.3m behind the targets. The acquired frequency band is between 10∼24GHz and the total number of frequencies is 201. The transmit/receive antennas synthesize a planar aperture of 1m×1m with a scanning step of 1cm. Classical synthetic aperture radar imaging algorithm for rectilinear configuration is applied using the acquired data to obtain 3D reconstructions of targets [24].

Figure 11 shows the obtained 1D range profiles of the two test targets from both uniform and the proposed nonuniform sampling method. With 201 frequency points, the MUR is 2.143m. Under uniform sampling, the ambiguity caused by the clutters from the wall appears at 1.4m, very close to the reflections of the targets. In contrast, the proposed weighted square-root sampling is able to significantly reduce the aliasing effects from clutters with no apparent response close to the target reflection. A flat ambiguity plateau caused by the targets starts to appear from 2.6m at the level of −20dB in comparison with the 0dB peak at 3.34m from uniform sampling. Under this sparse sampling scenario, the proposed nonuniform sampling method is able to drastically reduce the influence from clutters at larger distances while maintaining a relatively low level of ambiguities.

Figure 12 and 13 show the imaging results from the two targets under both uniform and nonuniform sparse sampling. Front and top view images are created by taking maximum values along the range and cross-range directions. In both cases, the ambiguity caused by the wall behind

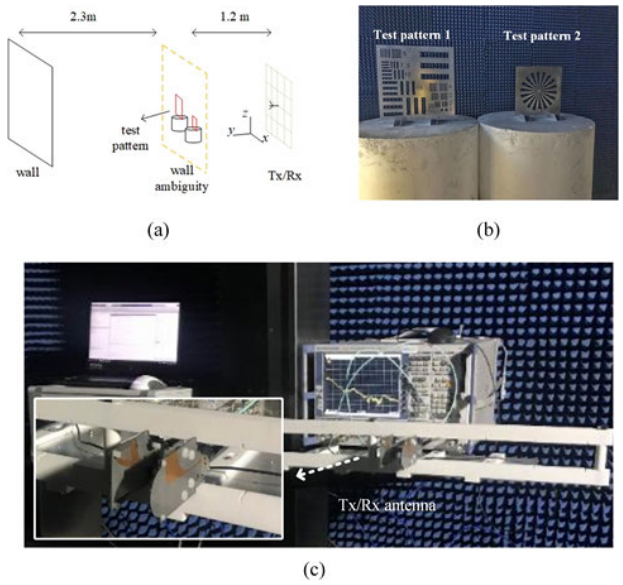

FIGURE 10. Experimental setup and measured test patterns. (a) The illustration of the measurement scenario where a wall is about 2.3m behind the test patterns, (b) the photo of the two test patterns. (test pattern 1 has slots with 1 ∼ 30mm width and separation, and the widest slot on target 2 is 2.5cm), (c) picture of the VNA and Vivaldi antennas used for the experiment.

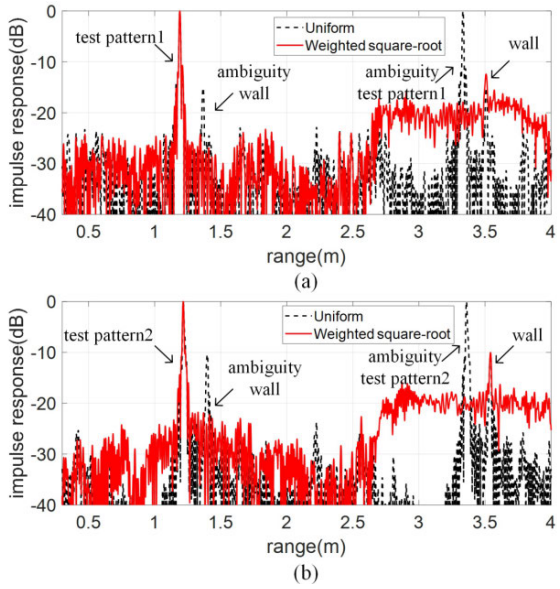

FIGURE 11. The measured 1D range profiles from uniform SFCW sweep and weighted square-root SFCW sweep.

the target creates a strong response close to the object under imaging. Since clutters are not controllable in real-life scenarios, it could easily overlap with the target response. In contrast, the proposed nonuniform frequency sampling strategy is very effective in suppressing ambiguities. The ratio between the responses from the targets and the clutters in the images is enlarged from 15dB to 30dB, while the resolution and image quality of the target are maintained without compromises.

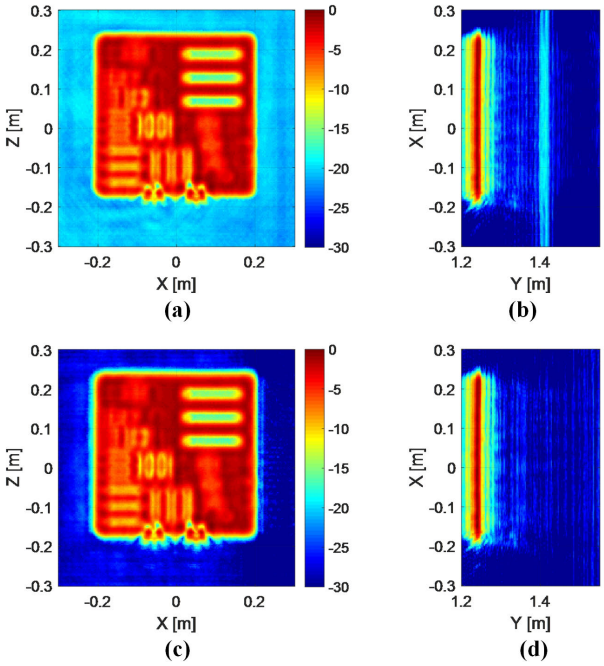

FIGURE 12. Comparison of imaging results of test pattern 1. (a),(b) show the front and top views from uniform frequency sampling, and (c),(d) show the front and top views from weighted square-root frequency sampling.

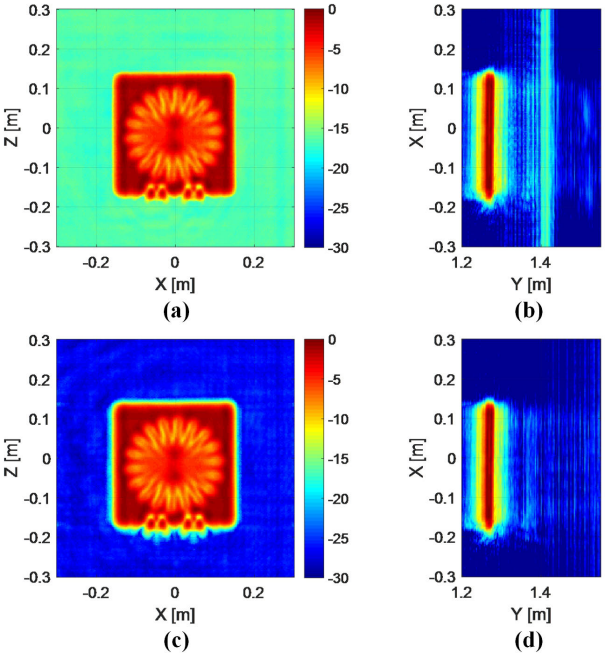

FIGURE 13. Comparison of imaging results of test pattern 2. (a),(b) show the front and top views from uniform frequency sampling, and (c),(d) show the front and top views from weighted square-root frequency sampling.

IV. CONCLUSION

In this paper, we propose a sparse nonuniform frequency sampling method which can effectively suppress range ambiguity from clutters in SFCW radar. A deterministic formula is derived using Poisson Sum formula for the purpose of choosing a discrete set of frequencies within

a specified frequency band. The corresponding frequency weighting formula is also formulated to maintain the same target impulse response in time-domain as the one achieved by uniform sampling. Both simulated and measurement results demonstrate the effectiveness of the proposed sparse sampling method in reducing aliasing effects under sparse sampling conditions. A ten-times reduction in the number of frequencies can be achieved with the proposed sparse sampling technique without visible compromise in the sensing and imaging performances. The proposed technique has the potential to significantly reduce acquisition time in SFCW, which is a key step in achieving real-time microwave/millimeter wave imaging.

ACKNOWLEDGMENT

The authors would like to thank Rohde and Schwarz China for their collaboration and support to our imaging experiments.

REFERENCES

[1] A. C. Gurbuz, J. H. McClellan, and W. R. Scott, "A compressive sensing data acquisition and imaging method for stepped frequency GPRs," *IEEE Trans. Signal Process.*, vol. 57, no. 7, pp. 2640–2650, Jul. 2009.
[2] L. Qu and T. Yang, "Investigation of Air/Ground reflection and antenna beamwidth for compressive sensing SFCW GPR migration imaging," *IEEE Trans. Geosci. Remote Sens.*, vol. 50, no. 8, pp. 3143–3149, Aug. 2012.
[3] S. Ahmed, A. Schiessl, F. Gumbmann, M. Tiebout, S. Methfessel, and L.-P. Schmidt, "Advanced microwave imaging," *IEEE Microw. Mag.*, vol. 13, no. 6, pp. 26–43, Sep. 2012.
[4] W. H. Weedon, W. C. Chew, and C. A. Ruwe, "Step-frequency radar imaging for nondestructive evaluation (NDE) and ground-penetrating radar (GPR) applications," *Proc. SPIE*, vol. 2275, Sep. 1994, Art. no. 186711.
[5] M. Pieraccini, D. Tarchi, H. Rudolf, D. Leva, G. Luzi, G. Bartoli, and C. Atzeni, "Structural static testing by interferometric synthetic radar," *NDT E Int.*, vol. 33, no. 8, pp. 565–570, Dec. 2000.
[6] S. R. J. Axelsson, "Analysis of random step frequency radar and comparison with experiments," *IEEE Trans. Geosci. Remote Sens.*, vol. 45, no. 4, pp. 890–904, Apr. 2007.
[7] A. Bayu Suksmono, E. Bharata, A. Andaya Lestari, A. G. Yarovoy, and L. P. Ligthart, "Compressive stepped-frequency continuous-wave ground-penetrating radar," *IEEE Geosci. Remote Sens. Lett.*, vol. 7, no. 4, pp. 665–669, Oct. 2010.
[8] J. Yang, J. Thompson, X. Huang, T. Jin, and Z. Zhou, "Random-frequency SAR imaging based on compressed sensing," *IEEE Trans. Geosci. Remote Sens.*, vol. 51, no. 2, pp. 983–994, Feb. 2013.
[9] W. Liu, C. Li, Z. Sun, Q. Zhang, and G. Fang, "Three-dimensional sparse image reconstruction for terahertz surface layer holography with random step frequency," *Opt. Lett.*, vol. 40, no. 14, p. 3384, Jul. 2015.
[10] P. P. Vaidyanathan and P. Pal, "Sparse sensing with co-prime samplers and arrays," *IEEE Trans. Signal Process.*, vol. 59, no. 2, pp. 573–586, Feb. 2011.
[11] G. Di Martino and A. Iodice, "Coprime synthetic aperture radar (CopSAR): A new acquisition mode for maritime surveillance," *IEEE Trans. Geosci. Remote Sens.*, vol. 53, no. 6, pp. 3110–3123, Jun. 2015.
[12] F. Gumbmann and A. Schiessl, "Short-range imaging system with a nonuniform SFCW approach," *IEEE Trans. Microw. Theory Techn.*, vol. 65, no. 4, pp. 1345–1354, Apr. 2017.
[13] A. Ishimaru, "Theory of unequally-spaced arrays," *IRE Trans. Antennas Propag.*, vol. 10, no. 6, pp. 691–702, Nov. 1962.
[14] A. Ishimaru and Y.-S. Chen, "Thinning and broadbanding antenna arrays by unequal spacings," *IEEE Trans. Antennas Propag.*, vol. 13, no. 1, pp. 34–42, Jan. 1965.
[15] Y. Chow, "On grating plateaux of nonuniformly spaced arrays," *IEEE Trans. Antennas Propag.*, vol. 13, no. 2, pp. 208–215, Mar. 1965.
[16] A. Ishimaru, "Unequally spaced arrays based on the Poisson sum formula," *IEEE Trans. Antennas Propag.*, vol. 62, no. 4, pp. 1549–1554, Apr. 2014.
[17] J. H. Doles and F. D. Benedict, "Broad-band array design using the asymptotic theory of unequally spaced arrays," *IEEE Trans. Antennas Propag.*, vol. 36, no. 1, pp. 27–33, Jan. 1988.
[18] J. Anton and A. Rockmore, "A unified approach to array-factor synthesis for line arrays with nonuniformly positioned elements," *IEEE J. Ocean. Eng.*, vol. 1, no. 1, pp. 14–21, Sep. 1976.
[19] H. Feshbach, P. M. Morse, and M. Michio, *Methods of Theoretical Physics*. New York, NY, USA: McGraw-Hill, 1953, p. 466.
[20] A. Papoulis, *Systems and Transforms With Applications in Optics*. New York, NY, USA: McGraw-Hill, 1968.
[21] A. Dutt and V. Rokhlin, "Fast Fourier transforms for nonequispaced data," *SIAM J. Sci. Comput.*, vol. 14, no. 6, pp. 1368–1393, Nov. 1993.
[22] L. Greengard and J.-Y. Lee, "Accelerating the nonuniform fast Fourier transform," *SIAM Rev.*, vol. 46, no. 3, pp. 443–454, Jan. 2004.
[23] J.-M. Lin, "Python non-uniform fast Fourier transform (PyNUFFT): An accelerated non-Cartesian MRI package on a heterogeneous platform (CPU/GPU)," *J. Imag.*, vol. 4, no. 3, p. 51, Mar. 2018.
[24] D. Sheen, D. Mcmakin, and T. Hall, "Near-field three-dimensional radar imaging techniques and applications," *Appl. Opt.*, vol. 49, no. 19, p. E83, Jul. 2010.
[25] X. Zhuge, A. G. Yarovoy, and L. P. Ligthart, "Circularly tapered antipodal Vivaldi antenna for array-based ultra-wideband near-field imaging," in *Proc. Eur. Radar Conf. (EuRAD)*, Sep./Oct. 2009, pp. 250–253.

WEIKANG SI received the B.S.E.E. degree from Zhengzhou University, Zhengzhou, China, in 2012, and the M.S.E.E. degree from the Beijing Institute of Technology, Beijing, China, in 2016. He is currently pursuing the Ph.D. degree with the School of Electronics and Information Engineering, Beihang University, Beijing.

His current research interests include microwave near-field measurement and imaging techniques.

XIAODONG ZHUGE was born in Beijing, China, in 1982. He received the M.Sc. and Ph.D. degrees *(Cum Laude)* from the Faculty of Electrical Engineering, Mathematics and Computer Science, Delft University of Technology, The Netherlands, in 2006 and 2010, respectively.

From 2011 to 2014, he was a Research Scientist with FEI Electron Optics, Eindhoven, The Netherlands. He was with the National Research Institute for Mathematics and Computer Science, The Netherlands, as a Researcher, from 2014 to 2017. Since 2017, he has been an Associate Professor with Beihang University, Beijing, where he leads a research team in the field of microwave and millimetre-wave sensing and systems, with a strong focus on near-field imaging and measurements.

Dr. Zhuge was a recipient of the Young Engineers Prize from the European Radar Conference in Munich, Germany, in 2007, and the Prestigious Veni Grant from the Netherlands Organization for Scientific Research (NWO), from 2014 to 2017.

JUNGANG MIAO received the B.S.E.E. degree from the National University of Defence Technology, Changsha, China, in 1982, the M.S.E.E. degree from Beihang University, Beijing, China, in 1987, and the Dr.rer.nat. degree in physics from the University of Bremen, Bremen, Germany, in 1998.

From 1982 to 1984, he was with the Institute of Remote Sensing Instrumentation, Chinese Aerospace, Beijing, where he developed space borne microwave remote sensing instruments. From 1984 to 1993, he was with the Electromagnetic Laboratory, Beihang University. In 1993, he joined the Institute of Environmental Physics and Remote Sensing, University of Bremen, as a Staff Member, where he was involved in the research on spaceborne microwave radiometry. Since 2003, he has been the Chair Professor with the Electromagnetic Laboratory, Beihang University. His current research interests include electromagnetic theory, microwave engineering, and microwave remote sensing of the atmosphere, including sensor development, calibration, and data analyses.